Circulation

ORIGINAL RESEARCH ARTICLE

LARP7 Protects Against Heart Failure by Enhancing Mitochondrial Biogenesis

Huijing Yu, PhD*
Fang Zhang, PhD*
Pengyi Yan, PhD*
Shasha Zhang, PhD*
⋮
Bing Zhang, MD, PhD

BACKGROUND: Heart failure (HF) is among the leading causes of morbidity and mortality, and its prevalence continues to rise. LARP7 (La ribonucleoprotein domain family member 7) is a master regulator that governs the DNA damage response and RNAPII (RNA polymerase II) pausing pathway, but its role in HF pathogenesis is incompletely understood.

METHODS: We assessed LARP7 expression in human HF and in nonhuman primate and mouse HF models. To study the function of LARP7 in heart, we generated global and cardiac-specific *LARP7* knockout mice. We acutely abolished LARP7 in mature cardiomyocytes by Cas9-mediated *LARP7* somatic knockout. We overexpressed LARP7 in cardiomyocytes using adeno-associated virus serotype 9 and ATM (ataxia telangiectasia mutated protein) inhibitor. The therapeutic potential of LARP7-regulated pathways in HF was tested in a mouse myocardial infarction model.

RESULTS: LARP7 was profoundly downregulated in failing human hearts and in nonhuman primate and murine hearts after myocardial infarction. Low LARP7 levels in failing hearts were linked to elevated reactive oxygen species, which activated the ATM-mediated DNA damage response pathway and promoted LARP7 ubiquitination and degradation. Constitutive *LARP7* knockout in mouse resulted in impaired mitochondrial biogenesis, myocardial hypoplasia, and midgestational lethality. Cardiac-specific inactivation resulted in defective mitochondrial biogenesis, impaired oxidative phosphorylation, elevated oxidative stress, and HF by 4 months of age. These abnormalities were accompanied by reduced SIRT1 (silent mating type information regulation 2 homolog 1) stability and deacetylase activity that impaired SIRT1-mediated transcription of genes for oxidative phosphorylation and energy metabolism and dampened cardiac function. Restoring LARP7 expression after myocardial infarction by either adeno-associated virus–mediated LARP7 expression or small molecule ATM inhibitor substantially improved the function of injured heart.

CONCLUSIONS: LARP7 is essential for mitochondrial biogenesis, energy production, and cardiac function by modulating SIRT1 homeostasis and activity. Reduction of LARP7 in diseased hearts owing to activation of the ATM pathway contributes to HF pathogenesis and restoring LARP7 in the injured heart confers myocardial protection. These results identify the ATM-LARP7-SIRT1 pathway as a target for therapeutic intervention in HF.

The full author list is available on page 2021.

*H. Yu, F. Zhang, P. Yan, and S. Zhang contributed equally.

Key Words: heart failure ■ mitochondria ■ oxidative stress

Sources of Funding, see page 2021

https://www.ahajournals.org/journal/circ

Clinical Perspective

What Is New?

- LARP7 (La ribonucleoprotein domain family member 7) is depleted in diseased myocardium from patients with heart failure and from rodent and nonhuman primate myocardial infarction models.
- LARP7 depletion in heart disease is mediated by elevated oxidative stress and its consequent activation of the ATM (ataxia telangiectasia mutated protein) DNA damage response pathway.
- Cardiomyocyte-specific knockout of *LARP7* reduces SIRT1 (silent mating type information regulation 2 homolog 1) activity, impairs mitochondrial biogenesis and oxidative respiration, and causes myocardial dysfunction.
- Restoration of LARP7 by adeno-associated virus 9–mediated gene therapy or by small molecule inhibition of ATM protects against myocardial dysfunction in mice after myocardial infarction.

What Are the Clinical Implications?

- LARP7 depletion is associated with the occurrence of heart failure.
- The ATM-LARP7-SIRT1 molecular axis is critical for maintaining energy metabolism and normal cardiac function.
- ATM-LARP7-SIRT1 dysfunction in heart failure exacerbates cardiac dysfunction.
- Normalizing the ATM-LARP7-Sirt1 pathway, either through small molecules or gene replacement therapy, may be a novel therapeutic approach to preserve function of the diseased heart.

Heart failure (HF), a clinical syndrome characterized by reduced heart function and an inability to pump sufficient blood and oxygen to meet the body's demands, is among the world's leading causes of morbidity and mortality, and its prevalence continues to rise. After decades of research, HF continues to carry a dismal prognosis, with 5-year mortality of ≈40% to 50%,[1,2] worse than that of many types of cancer. New therapeutic strategies are needed to combat this substantial and growing public health problem.

Mitochondria provide most of the energy required for the heart's pumping activity. A hallmark of HF is severe derangement of mitochondrial biogenesis and function, resulting in abnormally elevated oxidative stress. Mitochondrial biogenesis is controlled by SIRT1 (silent mating type information regulation 2 homolog 1), a type III histone deacetylase. SIRT1 physically interacts with and deacetylates PGC-1α (peroxisome proliferator-activated receptor γ coactivator 1α) at multiple lysine sites, which increases the transcription of genes for oxidative phosphorylation and thereby enhances oxygen consumption and energy production.[3] Under stress, SIRT1 deacetylates FOXO1/3 (forkhead box protein O) and induces expression of antioxidants of manganese-dependent superoxide dismutase and catalase, which mitigate oxidative stress and apoptosis and protect the heart from ischemia/reperfusion injury.[4–6] SIRT1 was recently revealed to increase SERCA2 (sarco-endoplasmic reticulum Ca^{2+}-ATPase) pump activity during HF by modulating the acetylation of SERCA2 at lysine 492.[7] SIRT1 protein and activity are significantly compromised in oxidative stress and HF, discovered by our and other groups.[6,8] The underling molecular mechanism has not been well clarified.

LARP7 (La ribonucleoprotein domain family member 7) is a La-related RNA binding protein associated with 7SK RNA with 1 RNA recognition motif and 1 HTH (helix-turn-helix) La-type binding domain, together with methylphosphate capping enzyme to maintain the integrity of 7SK ribonucleoprotein complex.[9,10] The major function of 7SK ribonucleoprotein described thus far is to limit RNAPII (RNA polymerase II), pausing release by sequestering positive transcription elongation factor b (P-TEFb).[10,11] Recently, we showed that LARP7 compromised the precise homology-directed DNA repair.[12] LARP7 is also a pivotal developmental regulator related with human genetic disease. For example, patients with LARP7 recessive loss-of-function mutations have Alazami syndrome, characterized by primordial dwarfism and intellectual disability.[13–15] However, LARP7 function in heart development and physiopathology has not been previously studied.

We initially unveiled in this study that LARP7 is downregulated in HF heart. To address the function of LARP7 in heart, we first generated *LARP7* constitutive knockout mouse that exhibited the defective heart development and HF and died prenatally. To further characterize the function of LARP7 in cardiomyocytes, we generated $NKX2.5^{Cre}$:$LARP7^{f/f}$ and Myh6Cre:$LARP7^{f/f}$ conditional knockout mice; both mouse strains developed HF with impaired mitochondrial morphology and function. The activation of ATM (ataxia telangiectasia mutated protein)–mediated DNA damage response (DDR) pathway on the oxidative stress accelerated the LARP7 decay that dampened the homeostasis and deacetylase activity of SIRT1 and consequently impaired the biogenesis of mitochondrial respiratory chain. Recovering LARP7 with either adeno-associated virus (AAV) serotype 9–mediated gene delivery or ATM inhibitor remarkably improved the pump function of infarcted heart and protected against HF. Together, these data uncover LARP7 as a novel gatekeeper to maintain the homeostasis of mitochondrial and cardiac function and underpin the molecular axis of ROS-ATM-LARP7-SIRT1 as a new therapeutic target for HF.

METHODS

Institutional review board approval of this study was obtained from Shanghai Jiao Tong University. All data are available within this article; raw and processed RNA sequencing data have also been made available at the GEO database (GSE155898) and can be assessed at https://www.ncbi.nlm.nih.gov/geo/query/acc.cgi?acc=GSE155898. The materials that support the findings of this study are available from the corresponding author on request.

Human Samples

Human control and dilated cardiomyopathy (DCM) hearts were collected at Tongji Hospital (Wuhan, China) as described previously,[16] following the principles outlined in the Declaration of Helsinki and with approval by the Ethics Review Board of Tongji Hospital and Tongji Medical College. Informed consents were signed by the patients or their medical proxies.

Animal Experiments

All animal protocol and procedures were approved by the Institute Animal Care and Use Committee of Shanghai Jiao Tong University. For echocardiographic studies and myocardial infarction (MI) surgeries, the operators were blinded from the animal genotypes, and animal numbers were estimated by the pilot experiments or published protocols.

Statistics

Statistical analyses were performed with GraphPad Prism and R. Data are presented as mean±SD unless otherwise noted. Two-tailed parametric *t* tests were used for 2-sample comparisons if the values were normally distributed. Otherwise, the Mann-Whitney *U* test was used. A 1-way analysis of variance with a Tukey post hoc test was used for comparisons among multiple groups. A Kaplan-Meier survival plot was deployed to evaluate MI mouse survival and log-rank test was used to calculate statistical differences. Values of $P<0.05$ were considered statistically significant.

RESULTS

LARP7 Depletion Led to Defective Mitochondrial Morphology and Heart Development

We found that LARP7 protein was significantly downregulated in 4 human DCM hearts compared with control hearts (normal hearts 0.77 versus HF 0.38, $P=0.013$; Figure 1A).[16] To gain insight into the function of LARP7 in heart, we generated *LARP7* conventional knockout mice (*LARP7*$^{-/-}$) using CRISPR technology. A microRNA cluster containing miR-302a through miR-302d and 367, embedded in the *LARP7* 8th intron, is expressed in the embryonic heart and reported to regulate heart development.[17] To avoid disturbing this microRNA cluster, we used CRISPR/Cas9 to specifically delete exons 2 and 3 in C57BL/6J mice (Figure IA and IB in the Data Supplement). Heterozygous *LARP7*$^{+/-}$ mice survived and reproduced normally, but homozygous *LARP7*$^{-/-}$ mice were not viable. We confirmed loss of LARP7 immunoreactivity in *LARP7*$^{-/-}$ embryos and normal expression of miR-302 and miR-367 (Figure IC and ID in the Data Supplement). Analysis of embryos at different stages of embryonic development indicated that *LARP7*$^{-/-}$ embryos died by E17.5. The knockout embryos were smaller than *LARP7*$^{+/-}$ or *LARP7*$^{+/+}$ littermate embryos, reminiscent of the primordial dwarfism phenotype observed in patients with *LARP7* mutations[14] (Figure 1B). Sections indicated hypoplasia of the compact myocardium at both E12.5 and E16.5 (Figure 1C). Atrial enlargement and lung compaction suggested congestive HF (Figure 1C). A subset of embryos also had ventricular septal defect, a type of congenital heart defect (Figure IC in the Data Supplement). These results indicate the mutagenesis of *LARP7* may be associated with congenital heart defect pathogenesis.

To investigate the mechanisms underlying abnormal development of the *LARP7*$^{-/-}$ heart, we examined myocardial ultrastructure by transmission electron microscopy. Compared with littermate controls, *LARP7*$^{-/-}$ cardiomyocytes had disorganized myofilaments. The Z-line was disorganized and faded and the I- and A-bands were indistinct. Although mitochondrial number was preserved, the mitochondria were smaller, the cristae were sparse and disarrayed, and empty vacuoles and broken membranes were observed frequently (Figure 1D and Figure IIA through IIC in the Data Supplement).

We analyzed the transcriptome of *LARP7*$^{+/+}$ and *LARP7*$^{-/-}$ hearts with RNA sequencing. A total of 260 genes were differentially expressed in *LARP7*$^{-/-}$ hearts (n=3; $P<0.05$; Figure IID through IIF and Table I in the Data Supplement). Gene ontology analysis indicated that these genes were enriched for functional terms pertaining to mitochondrial proton transport and oxidation reduction (Figure 1E). Many genes that encoded mitochondrial respiratory chain and inner membrane proteins were downregulated (Figure 1F). Defective oxidative respiration causes elevated oxidative stress, which was also observed in *LARP7*$^{-/-}$ cardiomyocytes, as assessed by increased 8-oxo-7,8-dihydroguanine (8-oxoG), the product of DNA oxidation (Figure IIIA and IIIB in the Data Supplement). There was also more cell death in *LARP7*$^{-/-}$ hearts (Figure IIIC and IIID in the Data Supplement). RNA sequencing indicated that angiogenesis was altered in *LARP7*$^{-/-}$ heart, but vessel-specific staining did not reveal significant alteration of vasculature (Figure 1E and Figure IIIE and IIIF in the Data Supplement).

Cardiomyocyte-Specific Deletion of LARP7 Resulted in DCM and HF

To further investigate the function of LARP7 in cardiomyocytes, we generated a LARP7 conditional allele (LARP7$^{f/f}$; Figure IVA and IVB in the Data Supplement).

ORIGINAL RESEARCH ARTICLE

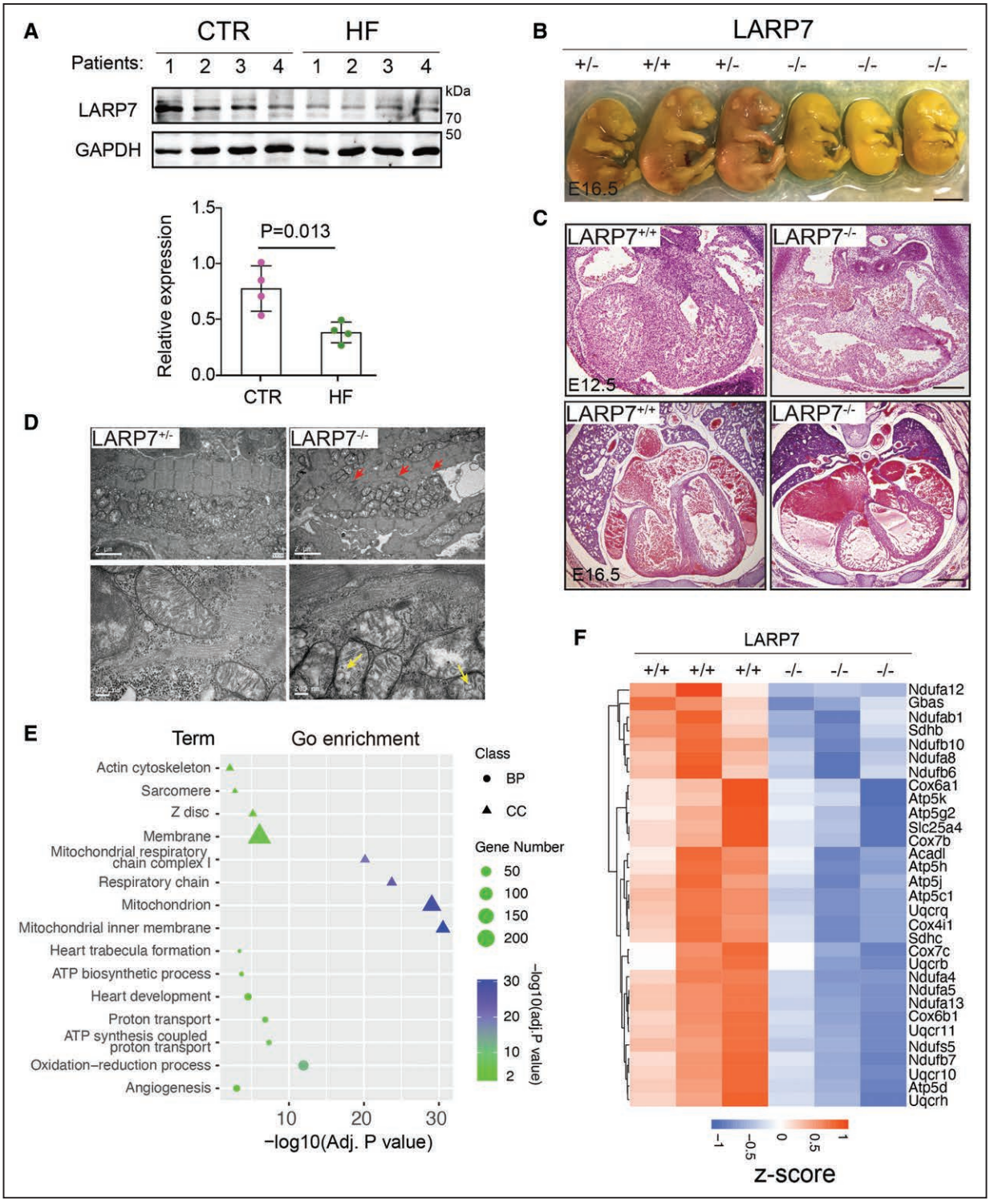

Figure 1. Constitutive knockout of LARP7 resulted in mitochondrial abnormality and developmental heart failure.
A, Western blotting shows that LARP7 expression is reduced in heart failure (HF [end-stage dilated cardiomyopathy with HF]) compared with normal hearts (CTR). The lower column plot quantifies the Western blotting by intensity normalized to glyceraldehyde 3-phosphate dehydrogenase (GAPDH; 2-tailed Student *t* test, n=4). **B**, Autopsy of *LARP7*$^{-/-}$ embryos at E16.5. The *LARP7*$^{-/-}$ embryos displayed global growth retardation (scale bar=500 mm). **C**, Hematoxylin & eosin staining demonstrates a HF syndrome with hypoplasia of myocardium, dilated atrium, and compacted lung (bottom right) in *LARP7*$^{-/-}$ embryos (scale bar=100 μm [E12.5] or 250 μm [E16.5]). **D**, Transmission electron microscopy images show the impaired mitochondrial morphology and disarrayed sarcomere in E16.5 cardiomyocytes. Statistical analysis is described in Figure IIA through IIC in the Data Supplement. Yellow arrows indicate the missing cristae and vacuole inside the mitochondrion. Red arrows indicate the faded and disarrayed sarcomeric structure. **E**, Gene ontology (Go) analysis of differentially expressed genes in the *LARP7*$^{-/-}$ heart. Genes of respiratory chain and proton transportation were preferentially affected by LARP7 deprivation as revealed by both biological process (BP) and cellular compartment (CC) analysis. **F**, RNA sequencing heat map shows electron transport chain complex genes downregulated in the E16.5 *LARP7*$^{-/-}$ heart compared with the *LARP7*$^{+/+}$ heart. Hierarchical algorithm was used for clustering. LARP7 indicates La ribonucleoprotein domain family member 7.

We used Myh6-Cre to specifically delete *LARP7* in cardiomyocytes (mCKO mice). Unlike *LARP7*$^{-/-}$ mice, mCKO mice survived to adulthood with a normal Mendelian ratio at weaning age (Figure IVC in the Data Supplement), indicating lack of significant fetal or perinatal loss. Serial measurement of heart function by echocardiography revealed that heart function of Myh6-Cre; LARP7$^{f/f}$ (mCKO) mice was similar to controls (LARP7$^{f/f}$ mice) at 2 months (Figure 2A and 2B and Figure VA in the Data Supplement), but by 4 months, the systolic function of mCKO mice was significantly impaired (control versus mCKO: ejection fraction 65.91±6.16 versus 48.31±6.81, *P*=0.00017; fraction shortening 35.27±4.95 versus 23.19±3.52, P=0.0001; detailed measurements in Table II in the Data Supplement) and the left ventricular internal diameter both in diastolic and systolic stage was profoundly increased (control versus mCKO: left ventricular internal diameter at end-diastole 3.68±0.23 versus 4.02±0.25, P=0.018; left ventricular internal diameter at end-systole: 2.34±0.30 versus 2.99±0.31, *P*=0.0011), disclosing enlarged chamber of mCKO heart (Figure 2A and 2B and Figure VA in the Data Supplement). The dissected hearts appeared larger with increased heart weight (*P*=0.0032; Figure 2C and 2D). Consistent with the echocardiography results, on histologic sections the mCKO hearts had enlarged left ventricular chambers and thinner myocardial walls (Figure 2E). Heart dysfunction and DCM phenotype were also reproduced in Nkx2-5$^{IRESCre/+}$; LARP7$^{f/f}$ (nCKO) mice, in which Nkx2-5^{IRESCre} directed LARP7 inactivation early in cardiogenesis (Figure VB–VE in the Data Supplement). Cardiomyocyte cross-sectional area, measured in tissue sections stained by wheat germ agglutinin, was significantly greater in mCKO compared with control hearts, suggesting that increased cardiomyocyte size contributed to the organ level cardiac enlargement (Figure 2F and 2G). Masson trichrome staining of 5-month-old hearts revealed excessive collagen deposition in mCKO hearts, indicating elevated cardiac fibrosis, a classic feature of pathologic cardiac remodeling (Figure 2H and 2I).

To gain further insight into whether LARP7 abrogation in adult heart could also impair cardiac function, we crossed our LARP7$^{f/f}$ mice with Myh6-MerCreMer mice to generate inducible *LARP7* knockout mouse Myh6-MerCreMer:LARP7$^{f/f}$ (*LARP7* iCKO). Two months after tamoxifen induction, echocardiography revealed reduced systolic function and increased chamber diameter in the iCKO hearts (Figure 2J and 2K and Figure VF in the Data Supplement). The iCKO hearts were significantly larger with increased heart weight (Figure 2L and 2M). Longitudinal sections of the hearts revealed enlarged ventricular chambers and slimmer walls, which were consistent with the echocardiographic results (Figure 2N). Together, these results suggest that LARP7 in the adult heart also has an essential role in maintaining cardiac homeostasis.

Abnormal Mitochondrial Morphology in *LARP7* Knockout Cardiomyocytes

Our studies of *LARP7*$^{-/-}$ embryos suggested that mitochondrial dysfunction may lead to HF in nCKO and mCKO mice. Therefore, we performed transmission electron microscopy on 4-month-old mCKO hearts and found that mCKO mitochondria were fewer, disorganized, and contained less cristae, similar to our observations of embryonic *LARP7*$^{-/-}$ cardiomyocytes (Figure 3A–3D and Figure VI in the Data Supplement). In comparison with *LARP7*$^{-/-}$ cardiomyocytes, mCKO cardiomyocytes processed fewer mitochondria. Reduced mitochondrial number was further validated by measuring mDNA to nDNA ratio using polymerase chain reaction (control versus mCKO: 1.00±0.17 versus 0.51±0.17, *P*=0.0022; Figure VIIA in the Data Supplement). Both lines of evidence together indicated defective mitochondrial biogenesis and function in cardiomyocytes lacking LARP7. HF itself could lead to the mitochondrial dysfunction and biogenesis.[18] Thus, we further assessed the mitochondrial ultrastructure by transmission electron microscopy in 1-month-old heart that had no apparent HF (Figure 3E–3H and Figure VIIB in the Data Supplement). The results demonstrated that even at this early HF-free stage, mitochondria already exhibited aberrant morphology, showing less mitochondria and dampened cristae. Mitochondrial DNA copy number was also decreased in 1-month-old mCKO heart, which was reversed by injection with AAV9–cardiac troponin T (cTnT)–LARP7 that expressed ectopic LARP7 in the cardiomyocyte (Figure VIIB in the Data Supplement). These results implicate LARP7 in enhancing mitochondrial biogenesis in the cardiomyocyte.

We further compared the mRNA expression profile of 4-month-old mCKO and wild-type hearts using RNA sequencing. Principal component analysis showed the gene expression profiles of mCKO hearts were distinct from control hearts (Figure VIIC in the Data Supplement), and 209 genes were differentially expressed in mCKO hearts (*P*<0.05; Figure VIID and VIIE in the Data Supplement). Many of them were tightly related to HF (Figure VIIF in the Data Supplement). For example, myosin heavy chain α (*Myh6*), the predominant myosin isoform of the adult mouse heart, cardiac troponin I (*Tnni3*), ATPase sarcoplasmic/endoplasmic reticulum Ca^{2+} transporting 2 (*Atp2a2*, also known as *Serca2*), and natriuretic peptides A (*Nppa*) and B (*Nppb*), biomarkers for HF, all declined, whereas fetal myosin heavy chain 7 (*Myh7*) and skeletal muscle actin α1 (*Acta1*) abnormally increased (Figure VIIF in the Data Supplement). Consistent with histologic evidence of cardiac fibrosis (Figure 2H), collagen genes *Col1a2*, *4a1*, *5a2*, and *6a2*

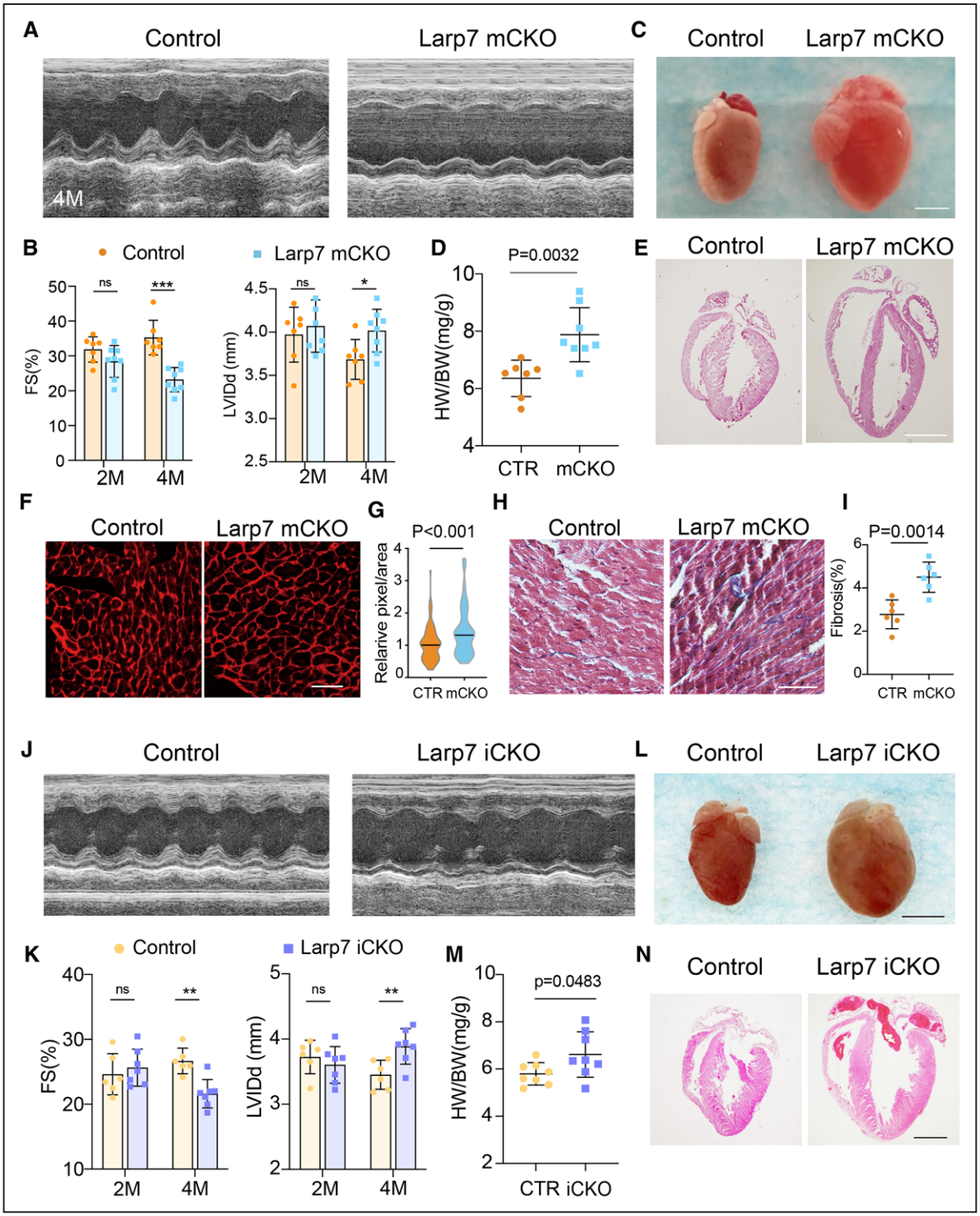

Figure 2. The cardiomyocyte-specific deletion of LARP7 led to dilated cardiomyopathy and heart failure in adult mouse.
A and **B**, M-mode echocardiogram illustrates reduced fraction shortening (FS) and increased left ventricle diastolic internal diameter (LVIDd) of Myh6-Cre; LARP7f/f (mCKO) hearts at 4 months (n=7 to 8, 2-tailed Student *t* test; **P*<0.05, ****P*<0.001). **C**, Representative anatomic images of wild-type and dilated mCKO hearts at 4 months (scale bar=2 mm). **D**, Ratio of heart weight (HW) to body weight (BW; control hearts [CTR], n=7; mCKO hearts, n=8; 2-tailed Student *t* test). **E**, Hematoxylin & eosin (HE) images of wild-type and mCKO heart. HE staining of sagittal section indicated dilated cardiomyopathy of mCKO heart (scale bar=2 mm). **F** and **G**, Increased cardiomyocyte size in 4-month-old mCKO hearts illustrated by wheat germ agglutinin staining. Violin plots represent 107 to 115 cardiomyocytes from 3 measured hearts (Mann-Whitney test; scale bar=20 μm). **H** and **I**, Increased collagen deposition in 5-month-old mCKO hearts. The fibrotic regions (blue) in 6 different fields per heart (6 hearts per group) were measured by ImageJ (2-tailed Student *t* test; scale bar=50 μm). **J** and **K**, Echocardiogram illustrates impaired FS and increased LVIDd of Myh6-MerCreMer; LARP7f/f (iCKO) hearts 2 months after tamoxifen induction. Myh6-MerCreMer:LARP7$^{f/f}$ mice were injected with 25 mg/kg/d tamoxifen (iCKO) for continuous 5 days at 2 months of age to deplete LARP7 from cardiomyocytes. Two-month-old MerCreMer mice with the same tamoxifen injection plan were used as controls (n=6 to 7; 2-tailed Student *t* test; ***P*<0.01). **L**, Representative gross anatomy of wild-type and dilated iCKO heart at 4 months of age (scale bar=4 mm). **M**, LARP7 iCKO mice had higher ratio of HW to BW (n=8; 2-tailed Student *t* test). **N**, HE staining shows the dilated cardiomyopathy of iCKO heart (scale bar, 1 mm). ns indicates no significance; and LARP7, La ribonucleoprotein domain family member 7.

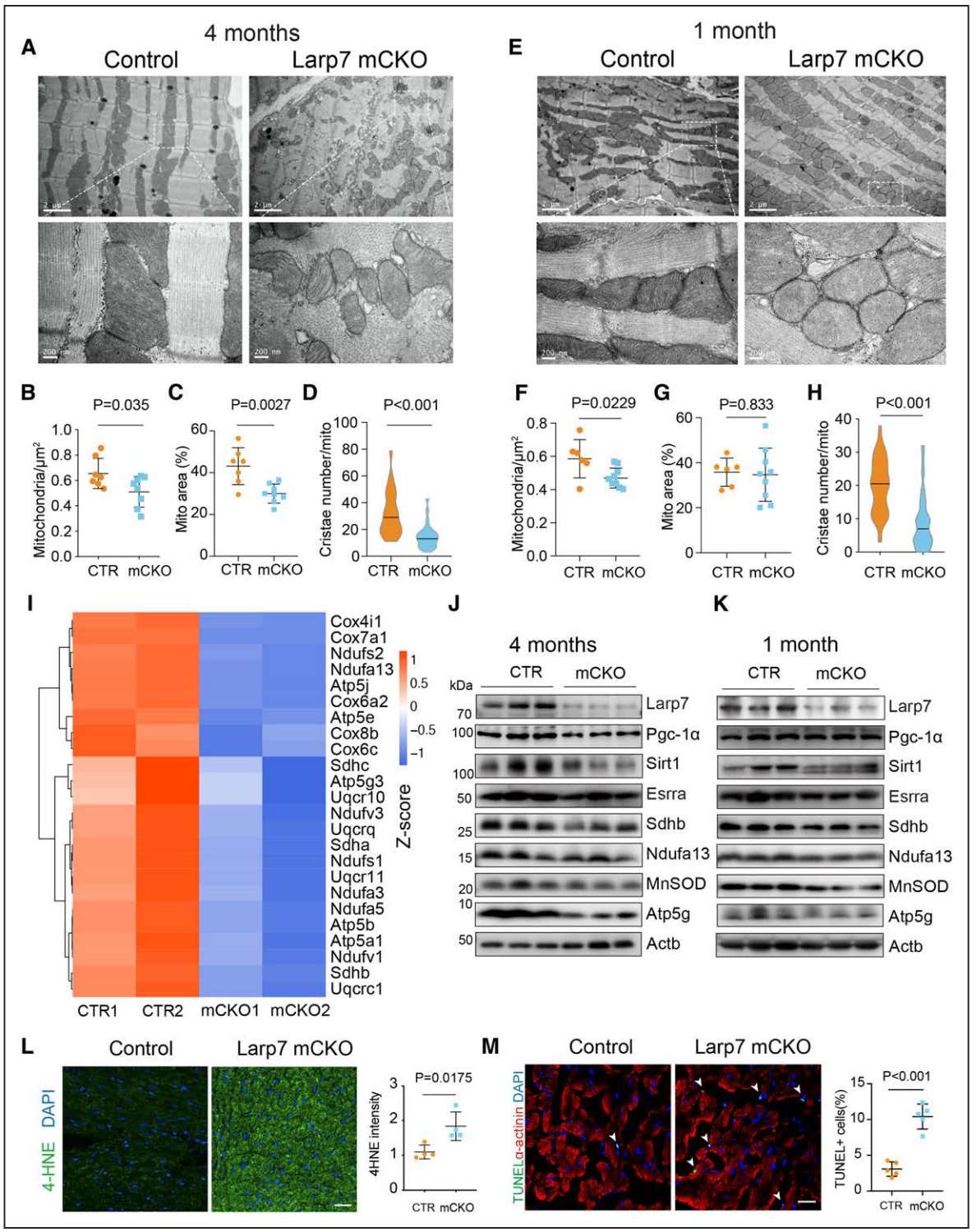

Figure 3. Impaired mitochondrial biogenesis in Myh6-Cre; LARP7$^{f/f}$ (mCKO) cardiomyocytes.
A through **D**, Cardiac ultrastructural assays show the impaired mitochondrial morphology in the 4-month-old mCKO heart. **A**, Representative transmission electron microscopy (TEM) images of control (CTR) and mCKO hearts. **B** through **D**, Quantifications of mitochondrial density (**B**), total area (**C**), and cristae number (**D**). More than 50 mitochondria in 3 mice for each group were measured (values are mean±SD; 2-tailed Student *t* test). **E** through **H**, TEM indicates early mitochondrial dysfunction in 1-month-old mCKO cardiomyocytes. **E**, Representative TEM images of 1-month-old cardiomyocytes. **F** through **H**, Quantification of mitochondrial density (**F**), total area (**G**), and cristae number (**H**; **F** and **G**, 2-tailed Student *t* test; **H**, Mann-Whitney *U* test; $P<0.05$ statistically significant). **I**, RNA sequencing heat map clustered in hierarchy shows that electron transport chain genes were downregulated in mCKO heart at 4 months. **J** and **K**, Western blotting of electron transport chain subunits and mitochondrial biogenic genes. Protein extracts from 4-month-old (**J**) and 1-month-old (**K**) heart apex were subjected to Western blot. **L**, 4-hydroxynonenal (4-HNE) staining unravels increased lipid peroxidation in mCKO heart, indicating elevated oxidative stress. 4-HNE fluorescent intensity was measured by ImageJ (**I**; n=4; mean±SD; 2-tailed Student *t* test; scale bar=25 μm). **M**, TUNEL assay (terminal deoxynucleotidyl transferase dUTP nick end labeling) shows more apoptotic cardiomyocytes in mCKO heart than in controls. Arrowheads denote the apoptotic cells (scale bar=25 μm; 4 mice; mean±SD; 2-tailed Student *t* test). DAPI indicates 4′,6-diamidino-2-phenylindole; and LARP7, La ribonucleoprotein domain family member 7.

increased profoundly in mCKO. Some of these gene expression changes were confirmed by quantitative real-time polymerase chain reaction (Figure VIIG in the Data Supplement). Myh6/Mhy7 ratio, an indication of fetal gene resurgence and pathologic remodeling, decreased sharply in mCKO heart (Figure VIIH in the Data Supplement). The alternative expression of HF indicators was also observed in the iCKO hearts, demonstrating that LARP7 depletion in the adult heart is able to induce HF (Figure VII and VIIJ in the Data Supplement).

A concordant downregulation of mitochondrial electron transport chain (ETC) genes was also observed (Figure 3I and Figure VIIL in the Data Supplement), which was further supported by gene set enrichment analysis (normalized enrichment score=–2.06, *P*=0.0051; Figure VIIK in the Data Supplement). The primary regulators for mitochondrial fusion/fission were not altered in mCKO heart or in the *LARP7*$^{-/-}$ heart, indicating that LARP7 deprivation may not affect the remodeling of mitochondrion (Figure VIIK and VIIL in the Data Supplement). Mitochondria biogenesis master regulator Pgc-1α, along with its coactivators Sirt1 and estrogen-related receptor α (ERRα), remained unchanged (Table I in the Data Supplement). We further evaluated the protein level of selected genes by Western blotting. This confirmed downregulation of ETC complex proteins NDUFA13 (NADH:ubiquinone oxidoreductase subunit A13), SDHB (succinate dehydrogenase complex iron sulfur subunit B), and ATP5G (ATP synthase, H^+ transporting, mitochondrial Fo complex, subunit C1), which were downregulated even more dramatically than their corresponding mRNAs. The master regulators of mitochondrial biogenesis SIRT1 and PGC-1α protein were both lower in 4-month-old mCKO hearts, whereas ERRα was equivalent to controls (Figure 3J). Analysis in 1-month-old hearts demonstrated that the ETC proteins and SIRT1 were already reduced at this early time point, whereas PGC-1α and ERRα were not (Figure 3K). These time-resolved results suggest that PGC-1α and ERRα downregulation may be a secondary effect of HF and that SIRT1 is directly downregulated by LARP7 mutation, a key mechanism by which LARP7 controls mitochondrial biogenesis and function. Further supporting the effect of SIRT1 downregulation in LARP7 mutants, superoxide dismutase 2 (manganese-dependent superoxide dismutase), a reactive oxygen species (ROS) scavenger that is transcriptionally controlled by SIRT1,[4–6] was downregulated in mCKO hearts (Figure 3J and 3K). Accordingly, ROS content increased in the mitochondria of isolated neonatal nCKO cardiomyocytes and in the mCKO adult heart tissue, as revealed by MitoSOX and 4-hydroxynonenal staining, respectively (Figure VIIIA in the Data Supplement and Figure 3L). Elevated myocardial ROS was associated with increased cardiomyocyte apoptosis in mCKO hearts (Figure 3M). MitoTEMPO, a specific scavenger for mitochondrial ROS, efficiently removed the ROS in the nCKO cardiomyocytes, improved heart function, and prevented the pathologic remodeling of mCKO hearts (Figure VIIIB–VIIIG in the Data Supplement). MitoTEMPO treatment did not change the expression of mitochondrial uncoupling proteins UCP2 and UCP3, indicating that the cardiac protection effect of MitoTEMPO was not through manipulating the mitochondrial uncoupling process (Figure VIIIH in the Data Supplement).

Defective Oxidative Phosphorylation in *LARP7* Knockout Mitochondria

Reduced expression of ETC complex subunits and PGC-1α suggested potential impairment of mitochondrial respiratory function in *LARP7*-knockout cardiomyocytes. To corroborate this hypothesis, we used an extracellular flux analyzer to assess mitochondrial function in isolated neonatal cardiomyocytes. nCKO cardiomyocytes had similar levels of basal respiration and proton leak compared with wild-type cardiomyocytes, but the maximal respiratory capacity and respiration attributed to basal F_1/F_0 ATP synthase activity were markedly reduced (Figure 4A and 4B and Figure IXA in the Data Supplement). In keeping with these data, the cellular ATP level of mCKO hearts was lower than that in controls (Figure 4C). To further corroborate the declined mitochondrial function in the adult *LARP7* knockout heart, we isolated the mitochondria from 1-month-old control and mCKO cardiac tissue and performed the coupling assay. The results demonstrated that the respiratory rate of state 3 and state 3u and the respiratory control ratio were significantly attenuated in the mCKO mice (Figure IXB–IXD in the Data Supplement). The activity of ETC complex I and IV coherently declined as well (Figure IXE and IXF in the Data Supplement). Together these results suggest that LARP7-deficient mitochondria have reduced ETC activity and impaired energy metabolism.

SIRT1 is a major regulator of mitochondrial biogenesis and energy metabolism and SIRT1 level was reduced in both young and old mCKO hearts (Figure 3J and 3K). To test the hypothesis that lower SIRT1 mechanistically contributes to mitochondrial dysfunction of LARP7-deficient cardiomyocytes, we measured the effect of reactivating SIRT1 in nCKO neonatal cardiomyocytes. Preadministration of the SIRT1-specific activator SRT1720 markedly improved maximal respiratory capacity of nCKO cardiomyocytes (Figure 4A and 4B). Impaired ETC activity was associated with relative mitochondrial depolarization in nCKO cardiomyocytes, and this was also normalized by SRT1720-induced SIRT1 activation (Figure 4D and 4E). Collectively, these results indicate that LARP7 controls mitochondrial function through SIRT1.

We next investigated whether upregulating LARP7 enhances mitochondrial oxidative phosphorylation. We ectopically expressed LARP7 in isolated cardiomyocytes

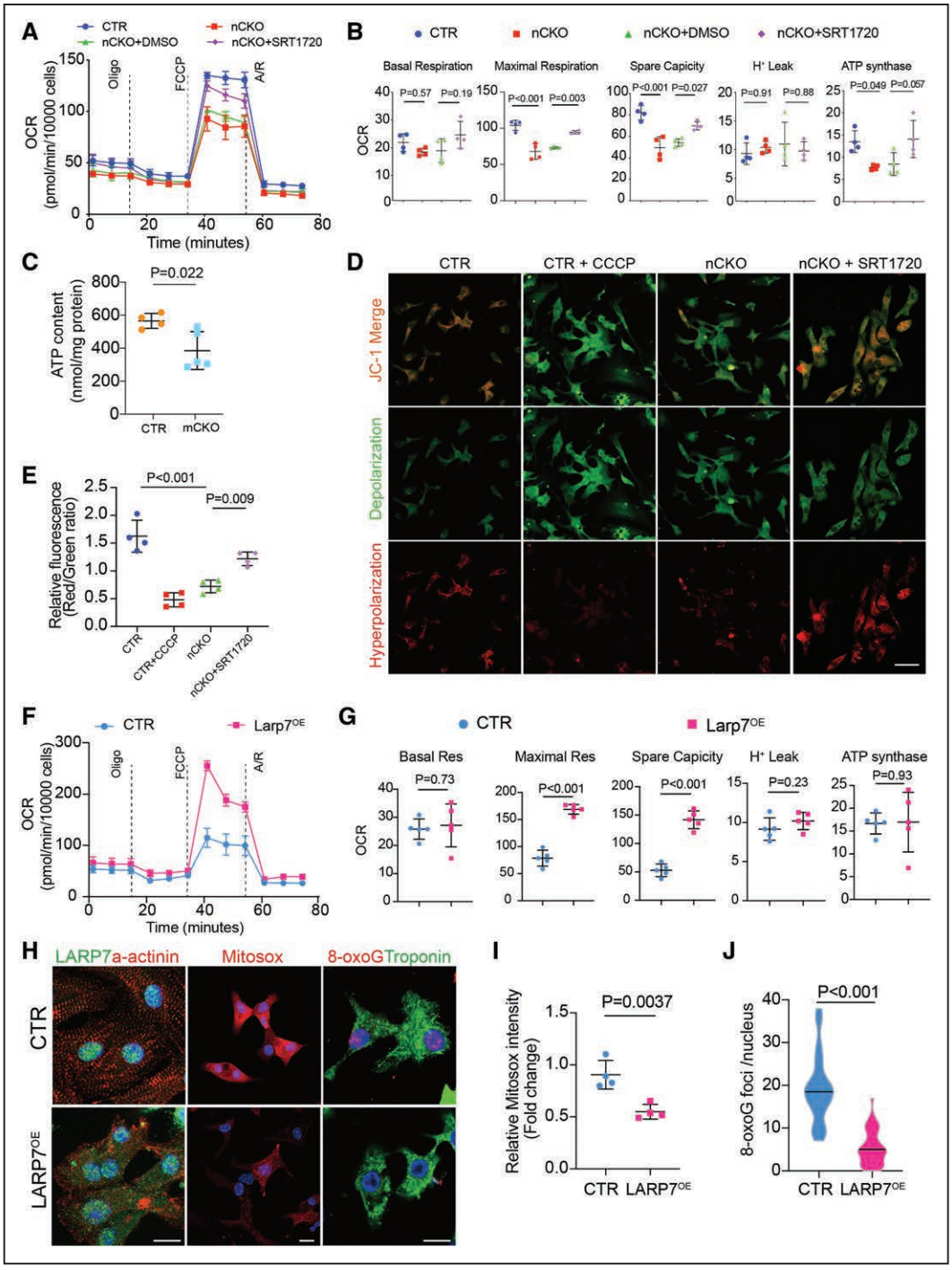

Figure 4. Defective oxidative phosphorylation and energy production in *LARP7* knockout cardiomyocytes.

A and **B**, Mitochondrial oxidative respiration decreased in Nkx2-5$^{IRESCre/+}$; LARP7$^{f/f}$ (nCKO) neonatal cardiomyocytes as assessed by measuring the cellular oxygen consumption rate (OCR). Shown are (**C**) time course data and (**D**) aggregated measurements from 4 independent assays; 0.5 μM SRT1720 and dimethyl sulfoxide (DMSO) were used in these assays. Definitions of basal respiration, spare respiration, H^+ leak, and ATP (adenosine triphosphate) synthesis are provided in Figure VIIA in the Data Supplement (data expressed as mean±SD; 1-way analysis of variance followed by Tukey multiple comparison test; statistically significant: $P<0.05$). **C**, ATP level in Myh6-Cre; LARP7$^{f/f}$ (mCKO) heart at 4 months (n=4 hearts in each group; 2-tailed Student *t* test). **D** and **E**, JC-1 staining measuring the mitochondrial membrane potential of isolated neonatal cardiomyocytes. There were increased depolarization (green) and decreased hyperpolarization (red) of mitochondria in nCKO neonatal cardiomyocytes, but treatment with 0.5 μM SRT1720 reversed them (**D**). Fifty-micrometer carbonyl cyanide 3-chlorophenylhydrazone (CCCP)–treated wild-type cardiomyocytes were presented as a positive control (CTR). Red/green fluorescence radio was measured from 4 independent repetitions (**E**; mean±SD; 1-way analysis of variance followed by Tukey multiple comparison test; statistically significant: $P<0.05$). **F** and **G**, Ad:LARP7 infection enhanced the mitochondrial spare and maximum respiration in wild-type neonatal cardiomyocytes. The time course data (**F**) represented 5 independent measurements (**G**). CTR, Ad:GFP; LARP7^{OE}, Ad:LARP7. Mean±SD, n=5, Two-tailed Student *t* test. **H** through **J**, LARP7 reduced reactive oxygen species burden in both mitochondria and nuclei. Mitochondrial reactive oxygen species was revealed by MitoSOX and nuclear reactive oxygen species by 8-oxo-7,8-dihydroguanine (8-oxoG; **H**). The data represent 4 independent stainings (**I** and **J**) and >30 cells in each group were counted for calculating 8-oxoG foci (**J**; scale bar=20 μm; mean±SD; n=4 experiments; 2-tailed Student *t* test). A/R indicates antimycin plus rotenone; FCCP, carbonyl cyanide-4 (trifluoromethoxy) phenylhydrazone; LARP7, La ribonucleoprotein domain family member 7; and Oligo, oligomycin.

using adenovirus. As expected, LARP7 overexpression increased ETC genes expression (Figure IXG in the Data Supplement) and dramatically improved both spare and maximal respiratory capacity but did not affect basal respiration, H^+ leak, or respiration attributed to basal F_1/F_0 ATP synthase activity (Figure 4F and 4G). LARP7 overexpression also reduced mitochondrial oxidative stress and DNA oxidation as measured by MitoSOX and 8-oxoG, respectively (Figure 4H–4J).

Reduced SIRT1 Contributes to Cardiac Dysfunction in LARP7 Loss of Function

We next sought to understand the contribution of the LARP7-SIRT1 axis to cardiac dysfunction in vivo. First we assessed whether LARP7 could directly modulate SIRT1 expressivity by acutely depleting LARP7 in the neonatal heart. We achieved neonatal LARP7 depletion using the CAS-AAV approach,[19] in which AAV and Cas9 are used to delete LARP7 in cardiomyocytes. We delivered AAV with cardiomyocyte-specific Cre and LARP7-targeting gRNA (AAV9-cTNT^{Cre}-U6-LARP7-sgRNA) into neonatal Rosa26fsCas9-dsRed mice. By 8 days after injection, LARP7 protein was efficiently depleted (Figure 5A). Consistent with LARP7 regulation of SIRT1 in mCKO heart, SIRT1 protein was also reduced (Figure 5A). We further confirmed the downregulation of nuclear SIRT1 protein in cardiomyocytes by immunofluorescent staining on isolating cardiomyocytes (Figure 5B and Figure XA in the Data Supplement). PGC-1α, which is directly deacetylated by SIRT1,[3] was more acetylated in LARP7 nCKO heart, which further indicated a declined SIRT1 deacetylase activity in addition to the protein deprivation (Figure 5C).

To test the hypothesis that SIRT1 downregulation was responsible for the mitochondrial and cardiac dysfunction of *LARP7* knockout hearts, we treated 2-month-old *LARP7* mCKO hearts with the SIRT1-specific activator SRT1720 (30 mg/kg) for 2 months (Figure 5D). At the end of the treatment period, SIRT1 activity was elevated ≈1.9-fold in mCKO heart (Figure XB in the Data Supplement). Compared with vehicle-treated mCKO hearts, SRT1720-treated mCKO hearts had significantly better systolic function (fraction shortening, mCKO+dimethyl sulfoxide [DMSO] versus mCKO+SRT1720: 20.95±2.95 versus 24.63±1.24, P=0.0376; Figure 5E) and reduced left ventricular diameter at end-diastole (mCKO+DMSO versus mCKO+SRT1720: 4.25±0.22 versus 3.89±0.19, P=0.0077; Figure 5E). These findings were further confirmed by necropsy showing reduced heart and left ventricular chamber size after SRT1720 treatment (Figure 5F). Cardiomyocyte hypertrophy and cardiac fibrosis observed in mCKO hearts were ameliorated (Figure XC and XD in the Data Supplement). Transmission electron microscopy demonstrated that mitochondrial number, size, and cristae structures and overall sarcomere structure in mCKO cardiomyocytes were improved but not fully corrected by SRT1720 (Figure 6G and Figure XE–XG in the Data Supplement).

ATM-DDR Mediated the Enhanced LARP7 Decay Under Oxidative Stress

We next sought to understand why LARP7 is downregulated in the failing heart. Our previous study demonstrated that activation of the ATM-DDR pathway downregulates LARP7.[12] ROS activates ATM-DDR pathways in diverse tissues including the heart.[20,21] Therefore, we hypothesized that LARP7 downregulation observed in the failing heart may arise from elevated ROS. We tested this hypothesis by treating isolated neonatal cardiomyocytes with 100 μm H_2O_2. H_2O_2 treatment rapidly increased ATM Ser1981 phosphorylation and substantially repressed LARP7 (Figure 6A). Quantitative real-time polymerase chain reaction illustrated that LARP7 mRNA levels were maintained across the entire time course (Figure 6B), indicating that protein reduction is posttranscriptional. Oxidative stress also changed the subcellular localization of LARP7: under basal conditions, LARP7 had predominant nuclear localization, and H_2O_2 resulted in almost complete loss of nuclear signal and increased signal within the cytoplasm (Figure 6C). Suppression of ROS with *N*-acetylcysteine recovered LARP7 nuclear localization and expression (Figure 6C). In mice, LARP7 protein decreased dramatically after birth, coinciding with elevated levels of oxidative stress that accompanied the transition to higher oxygen tension and greater reliance on oxidative phosphorylation[21] (Figure 6D). Moreover, treating neonatal mice with NAC increased LARP7 protein levels (Figure 6E). These results together suggest that elevated ROS mediates LARP7 degradation both in in vitro and in vivo models.

Next we investigated whether ROS-induced LARP7 degradation required ATM. Pretreatment of H9C2 cells, a cell line resembling rat embryonic cardiomyocytes, with ATM inhibitor KU60019 significantly blocked ATM phosphorylation and attenuated H_2O_2-induced downregulation of LARP7, as well as SIRT1 (Figure 6F). We previously showed that irradiation-induced ATM activation enhanced LARP7 polyubiquitination and degradation through the ubiquitin proteasome system. To test the hypothesis that ROS triggered LARP7 degradation through the same mechanism,[12] we measured LARP7 ubiquitination. ROS induced lysine 48 (K48)–linked polyubiquitination of LARP7, and this was abrogated by KU60019 (Figure 6G). Consistent with SIRT1 downregulation downstream of ROS- and ATM-mediated LARP7 depletion, KU60019 also reduced PGC-1α acetylation in H_2O_2-treated H9C2 cells (Figure 6H). Together, these data indicate that ATM links oxidative stress to LARP7 depletion and its downstream consequences.

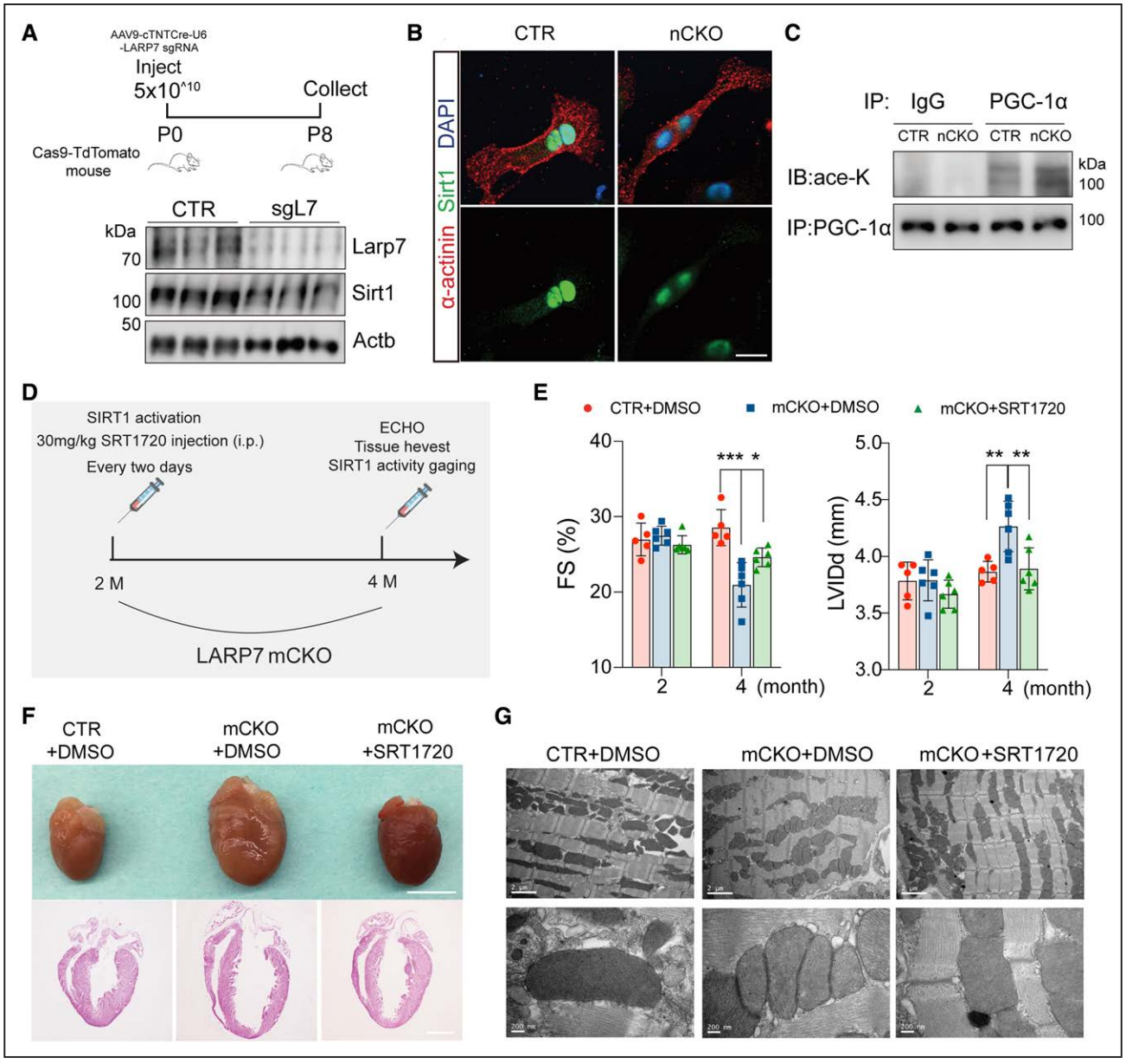

Figure 5. LARP7 deprivation dampened cardiac function by compromising SIRT1 deacetylase activity and homeostasis.
A, Transient LARP7 abrogation in neonatal heart using adeno-associated virus (AAV)–CAS approach repressed SIRT1. AAV9 expressing LARP7-specific sgRNA (AAV9-cTNT-Cre-U6-sgRNA) was injected to Rosa26-LSL-Cas9-tdTomato mouse at P0 to deplete LARP7 specifically in cardiomyocytes. LARP7 and SIRT1 protein were detected by Western blotting at P8. **B**, Immunofluorescent staining shows SIRT1 protein was repressed in the isolated P3 Nkx2-5$^{IRESCre/+}$; LARP7$^{f/f}$ (nCKO) cardiomyocytes (scale bar=20 μm). **C**, PGC-1α (peroxisome proliferator-activated receptor γ coactivator 1-α) acetylation was increased in nCKO neonatal heart. Total PGC-1α in neonatal heart was immunoprecipitated (IP) and then probed with lysine acetylation-specific antibody to reveal the acetylated PGC-1α. **D**, The dosing strategy for SRT1720 treatment: 30 mg/kg SRT1720 or only mock solvent (5% dimethyl sulfoxide [DMSO]+30% PEG300+H_2O) were intraperitoneally injected to Myh6-Cre; LARP7$^{f/f}$ (mCKO) mouse every 2 days for 2 months. **E**, Echocardiogram of SRT1720-treated mCKO mice. SRT1720 recovered the heart function of mCKO mice with increased fraction shortening (FS) and decreased left ventricle diastolic internal diameter (LVIDd) compared with mock injection (mean±SD; n=5 to 6; 1-way analysis of variance followed by a Tukey multiple comparison test; *P<0.05; **P<0.01; ***P<0.001). **F**, Gross anatomy and hematoxylin & eosin staining revealed SRT1720 ameliorated the dilation of mCKO heart at age 4 months (scale bar: 4 mm [upper]; 2 mm [lower]). **G**, Transmission electron microscopy shows SRT1720 ameliorated the malformation of mitochondria and contractile apparatus in mCKO cardiomyocytes. cTnT indicates cardiac troponin T; CTR, condition test ratio; DAPI, 4′,6-diamidino-2-phenylindole; IB, immunoblot; and IgG, immunoglobulin G; LARP7, La ribonucleoprotein domain family member 7; and SIRT1, silent mating type information regulation 2 homolog 1.

LARP7 Improved Myocardial Outcome After MI

We investigated the contribution of LARP7 downregulation to myocardial dysfunction after MI. We permanently ligated the left anterior descending coronary artery in 8- to 10-week-old male mice and measured the protein levels of LARP7, ETC subunits, SIRT1, and PGC-1α. Expression of these proteins was substantially reduced by 1 week after MI; in contrast, phosphorylated ATM was significantly elevated, indicating activation of the ATM-DDR pathway (Figure 7A). We performed

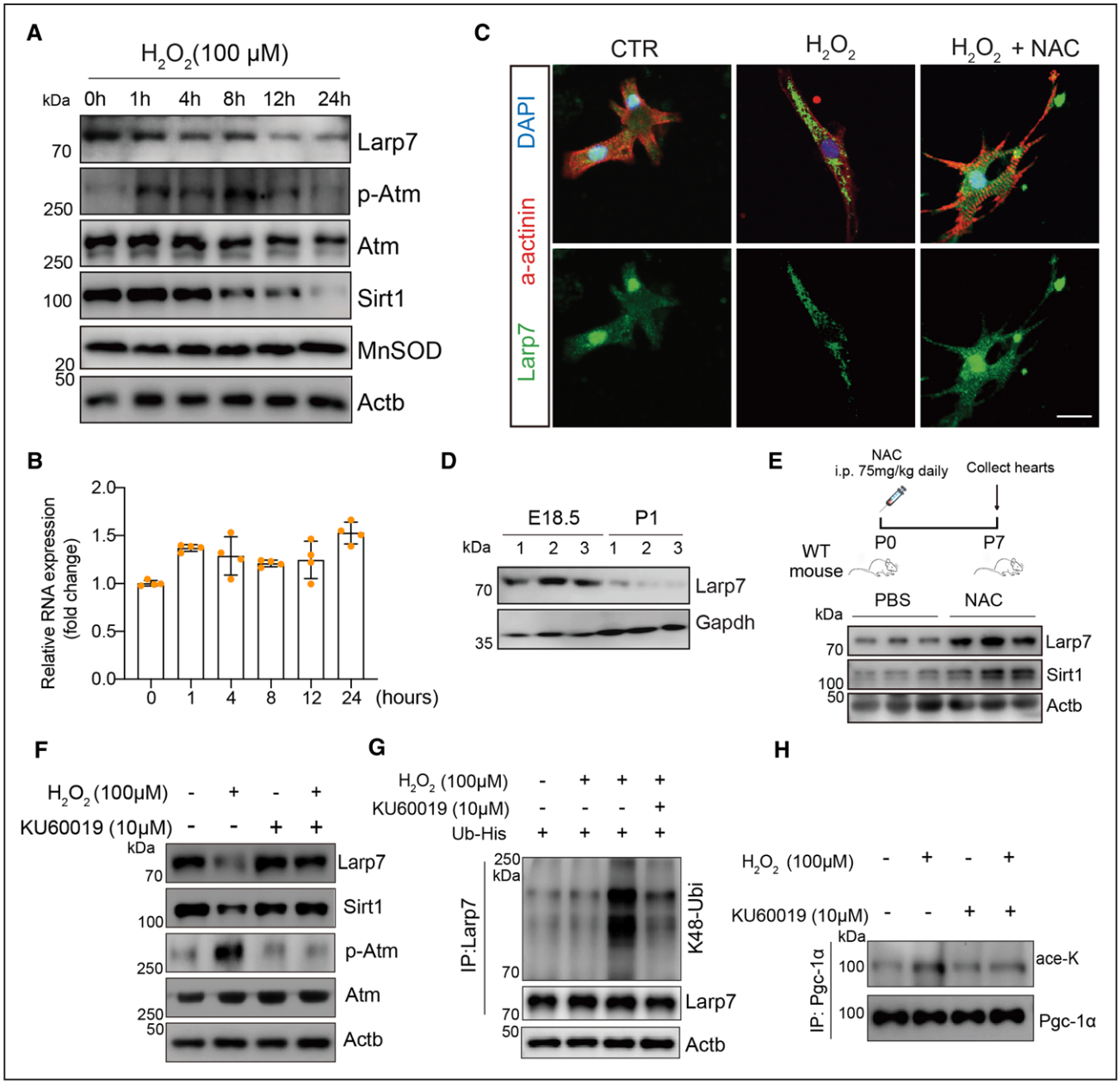

Figure 6. ROS enhanced LARP7 degradation by activating ATM–DNA DDR pathway.
A, Western blotting shows 100 μm H_2O_2 activated ATM kinase indicated by Ser1981 phosphorylation and repressed LARP7 and Sirt1 (silent mating type information regulation 2 homolog 1) in H9C2 cells. **B**, Reverse transcription polymerase chain reaction shows the H_2O_2 did not suppress LARP7 mRNA expression (mean±SD; n=4; 2-tailed Student *t* test). **C**, Immunofluorescent staining shows 2 hours of H_2O_2 treatment extranuclearly shuttled and decreased LARP7 in neonatal mouse cardiomyocytes and was blocked by 5-mM ROS scavenger NAC (scale bar=20 μm). **D**, Western blotting shows that LARP7 protein declined in neonatal hearts compared with embryonic hearts. **E**, N-acetylcysteine (NAC) restored LARP7 and SIRT1 in the neonatal hearts; 75 mg/kg NAC was injected to newborn mice for a week (n=3 each group). **F**, ATM inhibitor KU60019 blocked H_2O_2-induced ATM phosphorylation and attenuated LARP7 and SIRT1 degradation in H_9C_2 cells. **G**, H_2O_2 increased the polyubiquitination of LARP7, which was blocked by 10 μm KU60019. The polyubiquitinated LARP7 was pulled down by LARP7 antibody and then immunoblotted with the antibody specifically recognizing the K48-linked ubiquitination. **H**, Immunoprecipitation (IP) shows KU60019 blocked H_2O_2-induced PGC-1α acetylation in H_9C_2 cells. ATM indicates ataxia telangiectasia mutated protein; CTR, condition test ratio; DAPI, 4′,6-diamidino-2-phenylindole; DDR; damage response; LARP7, La ribonucleoprotein domain family member 7; PBS, phosphate-buffered saline; ROS, reactive oxygen species; and WT, wild-type.

parallel experiments in a nonhuman primate MI model. As in the murine model, permanent ligation of the left anterior descending coronary artery in 5- to 8-year-old cynomolgus monkeys[22] caused downregulation of LARP7, SIRT1, and mitochondrial respiratory proteins in infarcted hearts compared with sham-operated controls (Figure XIA in the Data Supplement). Together, these data indicate that ATM activation, LARP7 downregulation, and impaired mitochondrial biogenesis occur in experimental MI models, as well as in human HF (Figure 1A).

We performed the MI surgery on LARP7 iCKO mouse hearts 1 week after tamoxifen induction (Figure XIB and XIC in the Data Supplement). All the iCKO mice

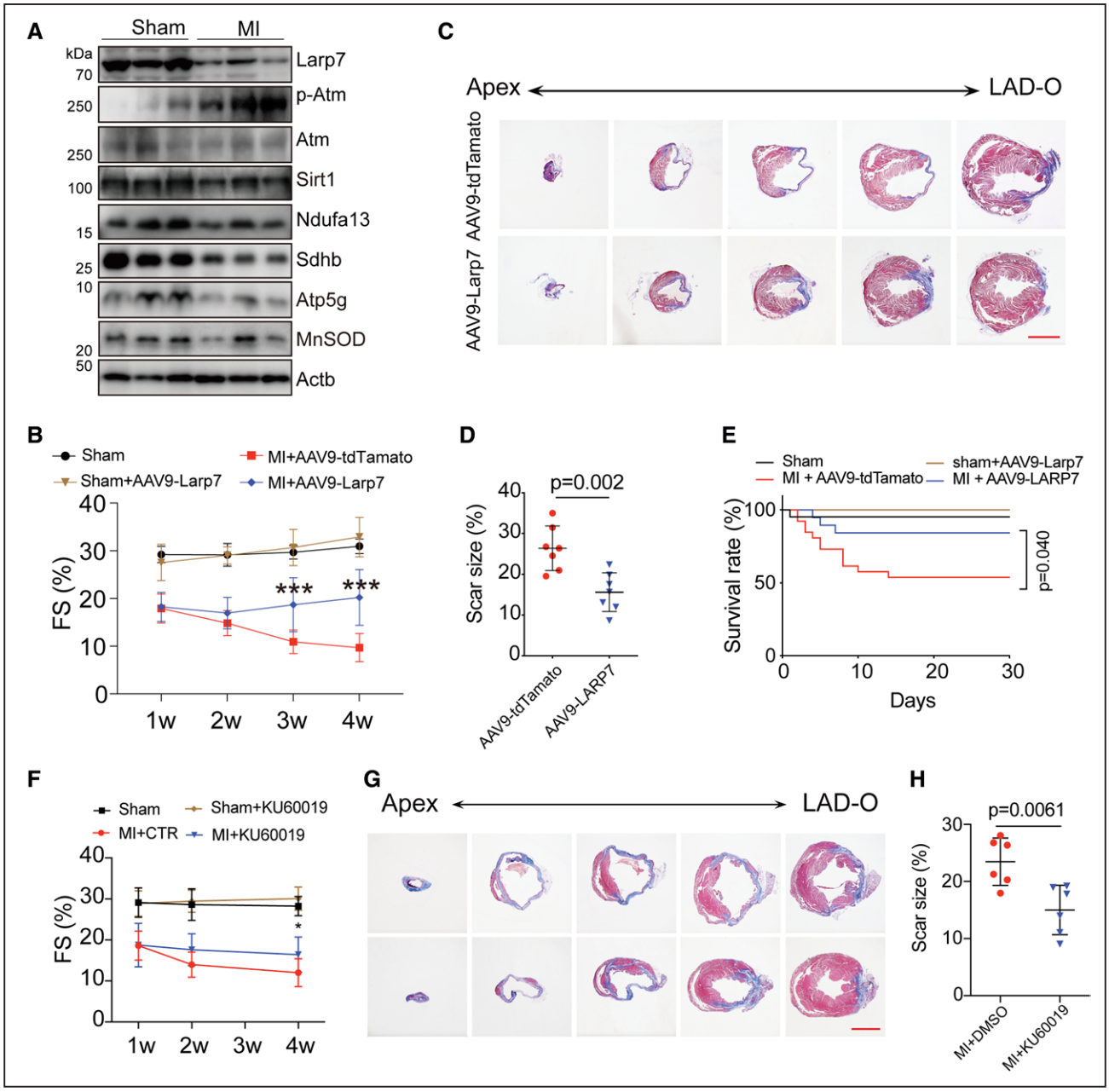

Figure 7. Restoration of LARP7 prevented heart failure after MI.

A, Western blotting of the myocardium remote to the infarction zone a week after MI. Declined LARP7, SIRT1 (silent mating type information regulation 2 homolog 1), and mitochondrial electron transport chain (ETC) genes and activated ATM (ataxia telangiectasia mutated protein) were observed in the MI heart. **B**, Systematic injection of adeno-associated virus 9 (AAV9)–cardiac troponin T (cTnT)–LARP7 restored fraction shortening (FS) of MI hearts 3 to 4 weeks after surgery (n=6 to 8 for sham and sham+sham+AAV9-LARP7; n=10 to 11 for MI+AAV9-taTamato and MI+AAV9-LARP7; ***P<0.001; mean±SD; 2-tailed Student t test). **C** and **D**, Trichrome staining of serial sections of MI heart. AAV9-cTNT-LARP7 injection reduced the scar size (the blue collagen region) of MI heart. Average scar sizes were calculated by ImageJ (**H**; n=7 per group; mean±SD; 2-tailed Student t test; scale bar=2 mm). **E**, Kaplan-Meier plot shows AAV9-LARP7 increased the survival rate of MI mice. Statistical significance was calculated with log-rank tests. **F**, Serial echography evaluates the function of MI hearts. Three weeks of KU60019 injection alleviated decline of the systolic function of MI heart (n=5 mice for sham and sham+KU60019; n=9 mice for MI and MI+KU60019). **G** and **H**, KU60019 reduced the scar size 1 month after MI. The scar size was revealed by trichrome stain (**G**) and calculated with ImageJ (**H**; scale bar=2 mm; n=6 per group; mean±SD; 2-tailed Student t test). DMSO indicates dimethyl sulfoxide; and LAD-O, left anterior descending coronary artery operation site; LARP7, La ribonucleoprotein domain family member 7; and MI, myocardial infarction.

(6/6) died within 1 week after MI; in comparison, only 2 control mice (out of 7) died within 1 month, indicative of a deteriorative response of iCKO hearts to the ischemic stress. To further interrogate whether LARP7 overexpression would improve the myocardial outcome after MI, we first systemically injected 5×10^{11} particles of AAV9-cTNT-LARP7 and AAV9-cTNT-TdTomato control virus through the tail vein 2 days before MI surgery (Figure XID in the Data Supplement). Mice were followed by echocardiography weekly until 1 month after MI, when hearts were collected and analyzed histologically. AAV9-cTNT-LARP7 significantly upregulated

LARP7 protein and prevented the decline of SIRT1 and ETC proteins after MI (Figure XIE in the Data Supplement). AAV9-cTNT-LARP7 improved overall survival of mice after MI (log-rank test: P=0.04; Figure 7F). Weekly echocardiography showed that the contractile function of AAV9-cTNT-TdTomato–treated hearts progressively declined. In contrast, the contractile function of AAV9-cTNT-LARP7–treated hearts partially recovered at 3 to 4 weeks (P<0.05; Figure 7B). Masson trichrome staining showed that AAV9-cTNT-LARP7 markedly reduced the MI scar size compared with AAV-cTNT-TdTomato control (Figure 7C and 7D).

Our data indicate that ATM mediates LARP7 downregulation in diseased cardiomyocytes, leading to the hypothesis that blocking ATM activation would prevent LARP7 degradation in cardiomyocytes and improve myocardial outcome after MI. To test this hypothesis, we treated mice with ATM inhibitor KU60019 1 day after MI surgery (Figure XIF in the Data Supplement). Consistent with the in vitro results (Figure 6F), KU60019 restored the expression of LARP7, SIRT1, and mitochondrial respiratory complex subunits in MI hearts (Figure XIG in the Data Supplement). Echocardiography showed that 3 weeks of KU60019 injection did not significantly affect the heart function of sham-operated mice, demonstrating that KU60019 at the dose we used did not have deleterious effects on the heart. However, in MI mice, KU60019 significantly attenuated the deterioration of systolic function, which is distinct to the untreated MI hearts (Figure 7F). Moreover, KU60019 treatment reduced the size of the infarcted region (Figure 7G and 7H).

Together, our results indicate that LARP7 restoration or ATM inhibition is an effective strategy to improve myocardial outcome after MI.

DISCUSSION

Our study highlights a pivotal role of LARP7 to control mitochondrial biogenesis and oxidative phosphorylation in heart homeostasis. We also demonstrate that LARP7 is downregulated in diseased hearts of patients and in experimental MI models in nonhuman primates and mice. Our data indicate that oxidative stress activates the ATM-mediated DDR pathway, which triggers LARP7 degradation. LARP7 downregulation or mutation reduces SIRT1 expression, causing greater PGC-1α acetylation and impairing mitochondrial biogenesis and energy metabolism. Ultimately this results in impaired cardiac function and contributes to the pathogenesis of HF. These lines of evidence define a new molecular pathway of ROS-ATM-LARP7-SIRT1 as a gatekeeper for maintaining the homeostasis of energy metabolism and cardiac function in the heart (Figure XII in the Data Supplement). Preventing the abnormal activation of this pathway protects the injured heart from dysfunction.

The DDR pathway senses genotoxic insults such as irradiation and genotoxic reagents and leads to cell cycle arrest and induction of DNA repair. ATM protein kinase is the principal mediator of the DDR.[23] ATM is activated by DNA double-strand breaks through MRN (Mre11-Rad50-Nbs1) DNA repair complex–mediated rapid intermolecular autophosphorylation of ATM at serine 1981.[23] A recent study demonstrated that oxidative stress like ROS activates ATM in human fibroblast cells, independent of DNA double-strand breaks and the MRN complex.[24] Our study demonstrates that ROS elevation in HF could also activate the ATM pathway in cardiomyocytes and causes LARP7 degradation as we showed in cancer lines treated with ionizing radiation and cisplatin.[12] Similar to our study, ROS-induced ATM activation also has been observed in the newborn and pressure overload–induced hypertrophic heart under excessive oxidative stress.[21,25]

The main function of activated ATM pathway mostly defined in cancer is to promote homology recombination by phosphorylating a broad spectrum of homology recombination–related proteins including H2AX and MRN (Mre11/Rad50/Nbs1).[23] The activation of ATM-mediated homology recombination enhances the healing of DNA double-strand breaks and prevents cells undergoing apoptosis, but also induces resistance to genotoxic treatment.[26] Beyond the canonical roles in DDR, ATM has been found to regulate aspects of metabolic syndrome such as insulin resistance and atherosclerosis.[27] A recent study by Nakada et al.[25] demonstrated that ATM pathway activation in response to overloading pressure promotes the expression of prohypertrophic genes and leads to deterioration in hypertrophic cardiomyopathy. We identify that ATM activation on oxidative stress in HF impairs mitochondrial biogenesis and energy production in cardiomyocytes and leads to cardiomyopathy and is attributed to the attenuation of LARP7-SIRT1 homeostasis. Prevention of ATM activation through ATM inhibitor protects the MI heart from HF, further underscoring the essence of this ROS-ATM-LARP7-SIRT1 axis in the pathogenesis of HF. It is well known that ROS is one of the major causes of cardiomyopathy. This newly defined molecular axis provides a novel mechanistic interpretation for ROS-induced cardiomyopathy.

A variety of ATM inhibitors have been developed to increase the sensitivity of chemoradiotherapies.[26] Combination treatment with ATM inhibitors and canonical chemoradiotherapies are being extensively tested in clinical trials. The promising efficacy of KU60019 in preserving heart function after MI as shown in our study provides the possibility to extend the applications of ATM inhibitors from the cancer therapy field to cardiomyopathy management. However, the ATM pathway harbors multiple critical biological functions in addition to what has been discussed in this article.

ATM mutagenesis results in a variety of clinical manifestations, such as neurologic degeneration, immunodeficiency, lymphoreticular malignancies, and premature ageing.[28,29] Although the safety of in vivo administration of an ATM inhibitor has been assessed by a number of studies as well as ours, long-term inhibition could cause unidentified severe adverse effects. In contrast, targeting LARP7, a downstream regulator of ATM, may provide better specificity and milder side effects than directly blocking ATM in preventing HF. Our data support this hypothesis by showing that myocyte-specific upregulation of LARP7 in MI hearts using AAV9-mediated delivery greatly improved cardiac function without showing any obvious adverse effects. AAV-based gene therapy within a certain range of doses has been proven safe for clinical use.[30] The AAV gene therapy drugs Luxturna (voretigene neparvovec) and Zolgensma (onasemnogene abeparvovec) were recently approved by the US Food and Drug Administration to treat RPE65-associated Leber congenital amaurosis and spinal muscular atrophy, respectively.[31,32] AAV-mediated LARP7 delivery may provide a promising target therapy for cardiac dysfunction.

CONCLUSIONS

This study demonstrated that a novel pathogenic pathway of ROS-LARP7-SIRT1-OXPHOS is responsible for HF. Correction of this pathway either with a gene therapy or small molecules approach presents promising therapeutic effects in a rodent model to improve cardiomyocyte function in HF. A large-scale trial in higher-profile mammal models such as minipigs or primates is warranted to further translate this bench discovery to a cure for HF.

ARTICLE INFORMATION

Received August 12, 2020; accepted February 17, 2021.

The Data Supplement is available with this article at https://www.ahajournals.org/doi/suppl/10.1161/circulationaha.120.050812.

Authors

Huijing Yu, PhD; Fang Zhang, PhD; Pengyi Yan, PhD; Shasha Zhang, PhD; Yingmei Lou, PhD; Zilong Geng, MD; Zixuan Li, MD; Yan Zhang, MD, PhD; Yuejuan Xu, PhD; Yanan Lu, MD; Chen Chen, PhD; Daowen Wang, MD; Wei Zhu, PhD; Xinyang Hu, MD, PhD; Jian'an Wang, MD; Tao Zhuang, PhD; Yuzhen Zhang, PhD; Gengze Wu, PhD; Junling Liu, PhD; Chunyu Zeng, PhD; William T. Pu, MD; Kun Sun, MD, PhD; Bing Zhang, MD, PhD

Correspondence

Bing Zhang, MD, PhD, Key Laboratory of Systems Biomedicine, Shanghai Center for Systems Biomedicine, Department of Pediatric Cardiology, Xin Hua Hospital, School of Medicine, Xin Hua Hospital, Shanghai Jiao Tong University, 800 Dong Chuan Rd, Shanghai, China, 200240. Email bingzhang@sjtu.edu.cn

Affiliations

Key Laboratory of Systems Biomedicine, Shanghai Center for Systems Biomedicine, Department of Pediatric Cardiology, Xin Hua Hospital, School of Medicine, Xin Hua Hospital, Shanghai Jiao Tong University, China (H.J.Y., F.Z., P.Y.Y., S.S.Z., Y.M.L., Z.L.G., Z.X.L., Y.J.X., Y.N.L., K.S., B.Z.). Renji-Med Clinical Stem Cell Research Center, Renji Hospital, School of Biomedical Engineering, Shanghai Jiao Tong University, China (Y.Z.). Division of Cardiology, Department of Internal Medicine, Tongji Hospital, Tongji Medical College, Huazhong University of Science and Technology, Wuhan, China (C.C., D.W.W.). Department of Cardiology, The Second Affiliated Hospital, School of Medicine, Zhejiang University, China (W.Z., X.Y.H., J.A.W.). Key Laboratory of Arrhythmias of the Ministry of Education of China, Research Center for Translational Medicine, Shanghai East Hospital, Tongji University School of Medicine, China (T.Z., Y.Z.Z.). Department of Cardiology, Chongqing Institute of Cardiology, Chongqing Cardiovascular Clinical Research Center, Daping Hospital, The Third Military Medical University, China (G.Z.W., C.Y.Z.). Department of Cardiology, Boston Children's Hospital, MA (W.T.P). Harvard Stem Cell Institute, Cambridge, MA (W.T.P).

Acknowledgments

The authors thank Guizhu Liu, Ying Yu, and Bin Zhou (Chinese Academy of Sciences, Shanghai Institutes for Biological Sciences), Jinghai Chen (Institute of Translational Medicine, Zhejiang University), Peng Zhan (First Affiliated Hospital, School of Medicine, Zhongshan University), and Yuxuan Guo and Qing Ma (William T. Pu Laboratory, Harvard Medical School) for technical assistance.

Sources of Funding

Dr Bing Zhang is funded by the National Key Research and Development Program of China (grants 2020YFA0803800, 2018YFC1312702, and 2018YFC1002400), National Science Foundation of China (grants 91539109, 31671503, 91939302, and 31872836), a Thousand Young Talents Award (16Z127060017), and the Innovation Program of the Shanghai Municipal Education Commission (2017-01-07-00-01-E0028).

Disclosures

None.

Supplemental Materials

Expanded Methods
Data Supplement Tables I–IV
Data Supplement Figures I–XII
References 32–38

REFERENCES

1. Askoxylakis V, Thieke C, Pleger ST, Most P, Tanner J, Lindel K, Katus HA, Debus J, Bischof M. Long-term survival of cancer patients compared to heart failure and stroke: a systematic review. *BMC Cancer.* 2010;10:105. doi: 10.1186/1471-2407-10-105
2. Braunwald E. Heart failure. *JACC Heart Fail.* 2013;1:1–20. doi: 10.1016/j.jchf.2012.10.002
3. Rodgers JT, Lerin C, Haas W, Gygi SP, Spiegelman BM, Puigserver P. Nutrient control of glucose homeostasis through a complex of PGC-1alpha and SIRT1. *Nature.* 2005;434:113–118. doi: 10.1038/nature03354
4. Brunet A, Sweeney LB, Sturgill JF, Chua KF, Greer PL, Lin Y, Tran H, Ross SE, Mostoslavsky R, Cohen HY, et al. Stress-dependent regulation of FOXO transcription factors by the SIRT1 deacetylase. *Science.* 2004;303:2011–2015. doi: 10.1126/science.1094637
5. Alcendor RR, Gao S, Zhai P, Zablocki D, Holle E, Yu X, Tian B, Wagner T, Vatner SF, Sadoshima J. Sirt1 regulates aging and resistance to oxidative stress in the heart. *Circ Res.* 2007;100:1512–1521. doi: 10.1161/01.RES.0000267723.65696.4a
6. Hsu CP, Zhai P, Yamamoto T, Maejima Y, Matsushima S, Hariharan N, Shao D, Takagi H, Oka S, Sadoshima J. Silent information regulator 1 protects the heart from ischemia/reperfusion. *Circulation.* 2010;122:2170–2182. doi: 10.1161/CIRCULATIONAHA.110.958033
7. Gorski PA, Jang SP, Jeong D, Lee A, Lee P, Oh JG, Chepurko V, Yang DK, Kwak TH, Eom SH, et al. Role of SIRT1 in modulating acetylation of the sarco-endoplasmic reticulum Ca2+-ATPase in heart failure. *Circ Res.* 2019;124:e63–e80. doi: 10.1161/CIRCRESAHA.118.313865
8. Kwon HS, Ott M. The ups and downs of SIRT1. *Trends Biochem Sci.* 2008;33:517–525. doi: 10.1016/j.tibs.2008.08.001
9. Uchikawa E, Natchiar KS, Han X, Proux F, Roblin P, Zhang E, Durand A, Klaholz BP, Dock-Bregeon AC. Structural insight into the mechanism of

stabilization of the 7SK small nuclear RNA by LARP7. *Nucleic Acids Res.* 2015;43:3373–3388. doi: 10.1093/nar/gkv173
10. Yang Z, Zhu Q, Luo K, Zhou Q. The 7SK small nuclear RNA inhibits the CDK9/cyclin T1 kinase to control transcription. *Nature.* 2001;414:317–322. doi: 10.1038/35104575
11. Krueger BJ, Jeronimo C, Roy BB, Bouchard A, Barrandon C, Byers SA, Searcey CE, Cooper JJ, Bensaude O, Cohen EA, et al. LARP7 is a stable component of the 7SK snRNP while P-TEFb, HEXIM1 and hnRNP A1 are reversibly associated. *Nucleic Acids Res.* 2008;36:2219–2229. doi: 10.1093/nar/gkn061
12. Zhang F, Yan P, Yu H, Le H, Li Z, Chen J, Liang X, Wang S, Wei W, Liu L, et al. L ARP7 is a BRCA1 ubiquitinase substrate and regulates genome stability and tumorigenesis. *Cell Rep.* 2020;32:107974. doi: 10.1016/j.celrep.2020.107974
13. Holohan B, Kim W, Lai TP, Hoshiyama H, Zhang N, Alazami AM, Wright WE, Meyn MS, Alkuraya FS, Shay JW. Impaired telomere maintenance in Alazami syndrome patients with LARP7 deficiency. *BMC Genomics.* 2016;17(suppl 9):749. doi: 10.1186/s12864-016-3093-4
14. Alazami AM, Al-Owain M, Alzahrani F, Shuaib T, Al-Shamrani H, Al-Falki YH, Al-Qahtani SM, Alsheddi T, Colak D, Alkuraya FS. Loss of function mutation in LARP7, chaperone of 7SK ncRNA, causes a syndrome of facial dysmorphism, intellectual disability, and primordial dwarfism. *Hum Mutat.* 2012;33:1429–1434. doi: 10.1002/humu.22175
15. Dateki S, Kitajima T, Kihara T, Watanabe S, Yoshiura KI, Moriuchi H. Novel compound heterozygous variants in the LARP7 gene in a patient with Alazami syndrome. *Hum Genome Var.* 2018;5:18014. doi: 10.1038/hgv.2018.14
16. Li H, Fan J, Zhao Y, Zhang X, Dai B, Zhan J, Yin Z, Nie X, Fu XD, Chen C, et al. Nuclear miR-320 mediates diabetes-induced cardiac dysfunction by activating transcription of fatty acid metabolic genes to cause lipotoxicity in the heart. *Circ Res.* 2019;125:1106–1120. doi: 10.1161/CIRCRESAHA.119.314898
17. Tian Y, Liu Y, Wang T, Zhou N, Kong J, Chen L, Snitow M, Morley M, Li D, Petrenko N, et al. A microRNA-Hippo pathway that promotes cardiomyocyte proliferation and cardiac regeneration in mice. *Sci Transl Med.* 2015;7:279ra38. doi: 10.1126/scitranslmed.3010841
18. Tsutsui H, Kinugawa S, Matsushima S. Oxidative stress and heart failure. *Am J Physiol Heart Circ Physiol.* 2011;301:H2181–H2190. doi: 10.1152/ajpheart.00554.2011
19. VanDusen NJ, Guo Y, Gu W, Pu WT. CASAAV: a CRISPR-based platform for rapid dissection of gene function in vivo. *Curr Protoc Mol Biol.* 2017;120:31.11.1–31.11.14. doi: 10.1002/cpmb.46
20. Nakada Y, Canseco DC, Thet S, Abdisalaam S, Asaithamby A, Santos CX, Shah AM, Zhang H, Faber JE, Kinter MT, et al. Hypoxia induces heart regeneration in adult mice. *Nature.* 2017;541:222–227. doi: 10.1038/nature20173
21. Puente BN, Kimura W, Muralidhar SA, Moon J, Amatruda JF, Phelps KL, Grinsfelder D, Rothermel BA, Chen R, Garcia JA, et al. The oxygen-rich postnatal environment induces cardiomyocyte cell-cycle arrest through DNA damage response. *Cell.* 2014;157:565–579. doi: 10.1016/j.cell.2014.03.032
22. Zhu K, Wu Q, Ni C, Zhang P, Zhong Z, Wu Y, Wang Y, Xu Y, Kong M, Cheng H, et al. Lack of remuscularization following transplantation of human embryonic stem cell-derived cardiovascular progenitor cells in infarcted nonhuman primates. *Circ Res.* 2018;122:958–969. doi: 10.1161/CIRCRESAHA.117.311578
23. Ciccia A, Elledge SJ. The DNA damage response: making it safe to play with knives. *Mol Cell.* 2010;40:179–204. doi: 10.1016/j.molcel.2010.09.019
24. Guo Z, Kozlov S, Lavin MF, Person MD, Paull TT. ATM activation by oxidative stress. *Science.* 2010;330:517–521. doi: 10.1126/science.1192912
25. Nakada Y, Nhi Nguyen NU, Xiao F, Savla JJ, Lam NT, Abdisalaam S, Bhattacharya S, Mukherjee S, Asaithamby A, Gillette TG, et al. DNA damage response mediates pressure overload-induced cardiomyocyte hypertrophy. *Circulation.* 2019;139:1237–1239. doi: 10.1161/CIRCULATIONAHA.118.034822
26. Weber AM, Ryan AJ. ATM and ATR as therapeutic targets in cancer. *Pharmacol Ther.* 2015;149:124–138. doi: 10.1016/j.pharmthera.2014.12.001
27. Schneider JG, Finck BN, Ren J, Standley KN, Takagi M, Maclean KH, Bernal-Mizrachi C, Muslin AJ, Kastan MB, Semenkovich CF. ATM-dependent suppression of stress signaling reduces vascular disease in metabolic syndrome. *Cell Metab.* 2006;4:377–389. doi: 10.1016/j.cmet.2006.10.002
28. Barlow C, Hirotsune S, Paylor R, Liyanage M, Eckhaus M, Collins F, Shiloh Y, Crawley JN, Ried T, Tagle D, et al. ATM-deficient mice: a paradigm of ataxia telangiectasia. *Cell.* 1996;86:159–171. doi: 10.1016/s0092-8674(00)80086-0
29. Sedgewick R, Boder E. Ataxia-telangiectasia. In: *Handbook of Clinical Neurology*. Elsevier Scientific Publishers; 1991:347–423.
30. Li C, Samulski RJ. Engineering adeno-associated virus vectors for gene therapy. *Nat Rev Genet.* 2020;21:255–272. doi: 10.1038/s41576-019-0205-4
31. Dunbar CE, High KA, Joung JK, Kohn DB, Ozawa K, Sadelain M. Gene therapy comes of age. *Science.* 2018;359:eaan4672. doi: 10.1126/science.aan4672
32. Keeler AM, Flotte TR. Recombinant adeno-associated virus gene therapy in light of Luxturna (and Zolgensma and Glybera): where are we, and how did we get here? *Annu Rev Virol.* 2019;6:601–621. doi: 10.1146/annurev-virology-092818-015530
33. Stanley EG, Biben C, Elefanty A, Barnett L, Koentgen F, Robb L, Harvey RP. Efficient Cre-mediated deletion in cardiac progenitor cells conferred by a 3'UTR-ires-Cre allele of the homeobox gene Nkx2-5. *Int J Dev Biol.* 2002;46:431–439.
34. Agah R, Frenkel PA, French BA, Michael LH, Overbeek PA, Schneider MD. Gene recombination in postmitotic cells: targeted expression of Cre recombinase provokes cardiac-restricted, site-specific rearrangement in adult ventricular muscle in vivo. *J Clin Invest.* 1997;100:169–179. doi: 10.1172/JCI119509
35. Sohal DS, Nghiem M, Crackower MA, Witt SA, Kimball TR, Tymitz KM, Penninger JM, Molkentin JD. Temporally regulated and tissue-specific gene manipulations in the adult and embryonic heart using a tamoxifen-inducible Cre protein. *Circ Res.* 2001;89:20–25. doi: 10.1161/hh1301.092687
36. Guo Y, VanDusen NJ, Zhang L, Gu W, Sethi I, Guatimosim S, Ma Q, Jardin BD, Ai Y, Zhang D, et al. Analysis of cardiac myocyte maturation using CASAAV, a platform for rapid dissection of cardiac myocyte gene function in vivo. *Circ Res.* 2017;120:1874–1888. doi: 10.1161/CIRCRESAHA.116.310283
37. Gao E, Lei YH, Shang X, Huang ZM, Zuo L, Boucher M, Fan Q, Chuprun JK, Ma XL, Koch WJ. A novel and efficient model of coronary artery ligation and myocardial infarction in the mouse. *Circ Res.* 2010;107:1445–1453. doi: 10.1161/CIRCRESAHA.110.223925
38. Frezza C, Cipolat S, Scorrano L. Organelle isolation: functional mitochondria from mouse liver, muscle and cultured fibroblasts. *Nat Protoc.* 2007;2:287–295. doi: 10.1038/nprot.2006.478